Influence of calcination on the sol-gel synthesis of lanthanum oxide nanoparticles

Kabir, Humayun; Nandyala, Sooraj Hussain; Rahman, M. Mahbubur; Kabir, Md Alamgir; Stamboulis, Artemis

DOI:
10.1007/s00339-018-2246-5

Applied Physics A

Influence of Calcination on Sol-Gel Synthesis of Lanthanum Oxide Nanoparticles

--Manuscript Draft--

Manuscript Number:	
Full Title:	Influence of Calcination on Sol-Gel Synthesis of Lanthanum Oxide Nanoparticles
Article Type:	Regular papers
Corresponding Author:	Humayun Kabir, MPhi; Jahangirnagar University Dhaka, Dhaka BANGLADESH
Corresponding Author Secondary Information:	
Corresponding Author's Institution:	Jahangirnagar University
Corresponding Author's Secondary Institution:	
First Author:	Humayun Kabir, MPhi;
First Author Secondary Information:	
Order of Authors:	Humayun Kabir, MPhi;
	Sooraj Hussain Nandyala, PhD
	M Mahbubur Rahman, PhD
	Md Alamgir Kabir, MRes
	Artemis Stamboulis, PhD
Order of Authors Secondary Information:	
Funding Information:	
Abstract:	A facile sol-gel technique was employed to synthesize Lanthanum Oxide nanoparticles (La2O3 NPs) effectively using micro-sized La2O3 powder, 20% nitric acid and high molecular weight polyethylene glycol (PEG) as starting materials and later their characteristics were studied via several characterization techniques, namely X-Ray diffraction (XRD), environmental scanning electron microscopy (ESEM), energy-dispersive X-ray spectroscopy, thermogravimetric analysis (TGA), differential scanning calorimetry (DSC), Fourier Transform infrared (FTIR) spectroscopy and photoluminescence (PL) spectroscopy. To investigate the influence of calcination temperatures on the particle size and other properties, the synthesized La2O3 nanopowder was calcined at several temperatures including 600 0C, 750 0C and 900 0C. The obtained results indicated that calcination temperatures affected significantly the crystallinity, particle size and lattice strain. The XRD patterns confirmed the hexagonal phase of the La2O3 NPs with lattice constant values, a = b = 0.3973 nm and c = 0.6129 nm. The average particle size of the La2O3 NPs estimated from ESEM images were in good agreement with the average crystal size obtained from the XRD data. The crystallinity as well as the mean crystallite size of the La2O3 NPs increased, while the lattice strain decreased with increasing calcinations temperatures. The Photoluminescence spectra of La2O3 NPs illustrated a strong emission band located at the wavelength of 364 nm which is typical green band and the wavelength of this band was not affected by the temperatures of the calcination.

Influence of Calcination on Sol-Gel Synthesis of Lanthanum Oxide Nanoparticles

Humayun Kabir[a, b], Sooraj Hussain Nandyala[a], M Mahbubur Rahman[b,c], Md Alamgir Kabir[a,b,d], Artemis Stamboulis[a]

[a]*School of Metallurgy and Materials, University of Birmingham, Edgbaston, Birmingham, B15 2TT, UK.*

[b]*Department of Physics, Jahangirnagar University, Savar, Dhaka-1342, Bangladesh.*

[c]*Surface Analysis & Materials Engineering Research Group*

School of Engineering & Information Technology, Murdoch University, Murdoch, WA 6150, Australia

[d]*Department of Physics, Kent State University , Kent, Ohio 44243, USA.*

Abstract:

A facile sol-gel technique was employed to synthesize Lanthanum Oxide nanoparticles (La_2O_3 NPs) effectively using micro-sized La_2O_3 powder, 20% nitric acid and high molecular weight polyethylene glycol (PEG) as starting materials and later their characteristics were studied via several characterization techniques, namely X-Ray diffraction (XRD), environmental scanning electron microscopy (ESEM), energy-dispersive X-ray spectroscopy, thermogravimetric analysis (TGA), differential scanning calorimetry (DSC), Fourier Transform infrared (FTIR) spectroscopy and photoluminescence (PL) spectroscopy. To investigate the influence of calcination temperatures on the particle size and other properties, the synthesized La_2O_3 nanopowder was calcined at several temperatures including 600 ^{0}C, 750 ^{0}C and 900 ^{0}C. The obtained results indicated that calcination temperatures affected significantly the crystallinity, particle size and lattice strain. The XRD patterns confirmed the hexagonal phase of the La_2O_3 NPs with lattice constant values, $a = b = 0.3973$ nm and $c = 0.6129$ nm. The average particle size of the La_2O_3 NPs estimated from ESEM images were in good agreement with the average crystal size obtained from the XRD data. The crystallinity as well as the mean crystallite size of the La_2O_3 NPs increased, while the lattice strain decreased with increasing calcinations temperatures. The Photoluminescence spectra of La_2O_3 NPs illustrated a strong emission band located at the wavelength of 364 nm which is typical green band and the wavelength of this band was not affected by the temperatures of the calcination.

Graphical Abstract

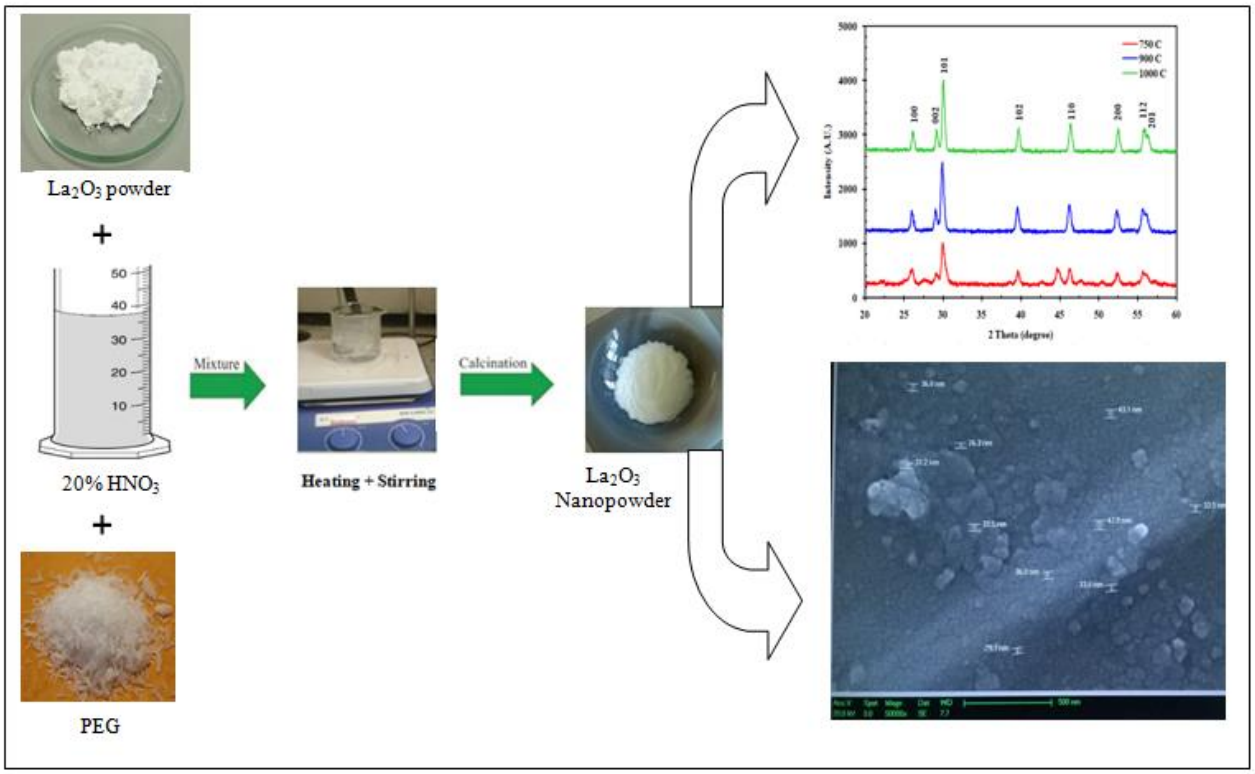

Key Words

Sol-gel technique, X-Ray diffraction, crystallinity, hexagonal phase, crystal size.

Corresponding Author Informations

Humayun Kabir [a,b]

rumy140@juniv.edu

[a]School of Metallurgy and Materials, University of Birmingham, Edgbaston, Birmingham, B15 2TT, UK.

[b]Department of Physics, Jahangirnagar University, Savar, Dhaka-1342, Bangladesh.

Highlights

- La_2O_3 NPs were synthesized successfully via a facile sol-gel technique.
- The calcination temperatures affected significantly the crystallinity, particle size and lattice strain.
- The crystallinity and the mean crystallite size of the La_2O_3 NPs increased, while the lattice strain decreased with increasing calcinations temperatures.

- The thermograms of all samples showed three main thermal transitions associated with weight loss.
- In PL spectra a strong emission band located at the wavelength of 364 nm is typical green band.

1. Introduction

Rare earth elements are distinguished by their high density, high melting point, high thermal conductance and conductivity. Because of their 4f orbital electron, they possess unique physical as well as chemical properties and have wide applications in electronics, medical, biomedical and agronomical fields [1, 2]. In plenty of areas of physics, chemistry, and materials science, metal oxides keep exceptionally significant contributions [3]. They can indicate metallic, semiconductor, or insulator character; because they can take an extensive number of structural geometries with a specific electronic structure. They have vast applications in technology, including fabrication of microelectronic circuits, sensors, piezoelectric devices, fuel cells, coatings against corrosion, and as catalysts. Metal oxides (MOs) are used as catalysts to prepare different products in chemical and petrochemical industries [4, 5]. They also used as catalysts or sorbents to carry away CO, NO_x, and SO_x species formed during the combustion of fossil fuels [5]. The greater portion of semiconductor industry uses of MOs to generate electronic components, like chips used in computers [6]. If the metal oxide's size is taken down to nanometer range, a number of properties depending on size initially develop because of surface chemistry [7-9]. As metal oxide nanoparticles (NPs) have confined size, so they can express unique chemical as well as physical properties. Particle size has impact on three momentous fundamental properties of a material. Firstly, the structural characteristics, exemplary lattice symmetry and unit cell parameters [10]. Normally, bulk MOs is stable with specific crystallographic structures. When the particle size decreases, the stability of thermodynamic as well as unit cell parameters alters and hence structural transformations may happen [11]. Secondly, particle size of MOs is connected to the electronic properties. If the size of particle reduces, the energy of exciton levels of a semiconductor MOs displaces and therefore the optical band gap of the MOs varies [12]. When the structural and electronic properties of MOs vary, they evidently switch the physical as well as chemical properties of a MOs. This is the third group of characteristics that is dominated by the size of the particles [13].

Lanthanum (III) oxide, La_2O_3, called lanthania is an odourless, white solid and is a rare earth metal oxide. Lanthania is not soluble in water, but soluble in dilute acid. La_2O_3 has the greatest

optical band gap of the rare earth oxides, 4.3 eV, the minimum lattice energy and an extremely high dielectric constant, 27 [14]. Because of these interesting properties, lanthania has a lot of potential applications in different cases, for instance fuel cells, dielectric layers in devices, optics, magnetic data storage and magnetic resonance imaging (MPI), ceramics, gas sensors, catalysis, automobiles, biosensors, automobiles, water treatment, biomedicine, protective and optical coating, preparing several perovskite nanostructures, photoelectric conversion, optical filters, light converting agricultural films, in light emitting materials (blue powder), for preparing high refraction optical fibres, precision optical glasses and other alloys materials, etc. [15-19]. A several methods have developed for the synthesizing of La_2O_3 ultrafine powders, nanopowders, nanorods, nanowires, nanosheets, nanoneedles, nanobundles and nanoparticles, incorporate with sol–gel [20, 21], hydrothermal [22, 23], sonochemical [24, 25], microwave [26], solvo-thermal [27], laser deposition [28], thermal decomposition [29], chemical precipitation [30], reveres micelles [31], arc-discharge [32], green carbonation [33], starch template [34] and other chemical and physical techniques. All these methods have their own advantages and disadvantages. Amongst these methods, the sol-gel synthesis process is a facile, inexpensive and does not require any specialist equipment. Goharshadi *et al.* synthesized lanthania nanoparticles [35] using $LaCl_3$, $7H_2O$ as the starting materials, ammonia solution as hydrolysis agents and hexadecyltrimethyl ammonium bromide as a surfactant using hydrothermal process. The obtained average particle size was below 30 nm. La_2O_3 NPs were also prepared by Nejad *et al.* using same process starting from lanthanum nitrate, $La(NO_3)$. $6H_2O$ and the obtained mean particle size was around 50 nm [22]. A simple sol–gel method has been employed by Wang *et al.* [36] to synthesis La_2O_3 nanoparticles by mixing commercial powder La_2O_3, polyethylene glycol (PEG) and nitric acid. They showed that particle size is strongly influenced by calcination temperature as well as concentration of PEG in the solution. The average particle size of La_2O_3NPs decreased with increasing PEG concentration. Niasari *et al.* studied the synthesis of lanthanum carbonate, $La_2(CO_3)_3$ for the preparation of $La(OH)_3$ and La_2O_3 NPs via sonochemical method [37]. They reported the variation of surfactant, calcination temperature as well as sonication time on the morphology and particle size of the NPs and concluded that sonication time of 30 min and calcination temperature of 600 ^oC are optimum condition to synthesize $La_2(CO_3)_3$ and La_2O_3, respectively and addition of surfactant is not required. Synthesis of nanostructure La_2O_3 as a heterogeneous catalyst has been reported by Zhou *et al.* [38] via sonochemical technique for biodiesel synthesis.

In this study, we reported surfactant assisted sol-gel technique to synthesis La_2O_3 NPs using surfactant PEG as template agent and micro-sized lanthanum oxide powder as precursors. As-synthesized products were characterized by XRD, ESEM, TGA, DSC, PL and FTIR spectroscopy. The influence of calcination temperatures on average particle size was also

investigated. A deeper understanding the properties and the synthesis technique will be useful for developing the potential applications of La_2O_3 NPs.

2. Experimental details

2.1 Raw materials and synthesis process La_2O_3 NPs

All the chemical reagents used in this synthesis process were analytical grade, purchased from Sigma Aldrich, UK, and were used as direct without further purification.

In this synthesis process, the sol-gel technique was used to prepare La_2O_3 NPs. In a typical process, 2.00 g micro-sized (≈300 μm) commercially purchased La_2O_3 powder was kept in a pre-cleaned glass beaker. The required amount (≈18.5 ml) of 20% aqueous solution of HNO_3 was added drop wise to the La_2O_3 powder with continuous and vigorous magnetic stirring until all La_2O_3 powder reacted with HNO_3 to produce an aqueous solution of lanthanum nitrate ($La(NO_3)_3$. $6H_2O$). Then various amounts of PEG were added to produce a solution with different PEG concentrations, such as 30 g/l, 40 g/l, 45 g/l, 50 g/l, 60 g/l and 70 g/l. The solution was then further stirred for 15 minutes using a magnetic stirrer. The solution was then kept in a water bath at 80 °C with continuous stirring for approximately 2.0 hours until most of the water was evaporated and a clear gel was formed. The obtained product was allowed to cool down to room temperature. The whole experimental procedure was carried out in the fume cupboard for safety reasons. Thereafter, the product (clear gel) was placed in an oven at 90 °C for 72 h to obtain a dry gel. The dry gel was then grounded using an agate mortar and pestle to obtain a white powder. In order to remove the organic phase and decompose the $La(NO_3)_3$, the powder was heat treated in a furnace at 300 °C. Eventually, the resultant powder was calcined at the several temperatures including 750 °C, 900 °C, and 1000 °C. The final product was La_2O_3 NPs. The flow chart for the preparation of La_2O_3 NPs via the sol-gel technique is illustrated in Fig. 1. Within six trial samples, best three samples (PEG concentration: 30 g/l, 45 g/l and 60 g/l0) in each calcination temperature, such as 750 ^{0}C, 900 ^{0}C and 1000 ^{0}C were taken for different measurements.

2.2 Characterization of Samples

An Equinox 3000 X-ray powder diffractometer was used to perform the structural characterization of the as synthesised La_2O_3 NPs in the 2θ range from 10^o to 60^o, and step of 0.03^0, with graphite monochromatic Cu Kα radiation (λ = 0.154 18 nm). The operating voltage and current was 35 kV and 25 mA, respectively. The surface morphology of all NPs samples was investigated using a Philips XL 30 ESEM equipped with Oxford INCA EDX FEG electron microscope operated at 20 kV at different magnifications. Specimens were prepared by dispersing

La_2O_3 NPs in absolute ethanol under ultra-sonication, dropping a little solution onto thin Cu coating film which was set previously on a steel stab and evaporating the solvent naturally in air. Then resulting specimens were sputter coated with a thin layer of platinum in vacuum. The EDS of the samples was performed by a Philips XL 30 ESEM and EDX FEG electron microscope operated at 10 kV. The FTIR spectra were recorded in transmittance (%) mode at room temperature by using a double beam IR spectrophotometer (Nicolet 8600 FTIR spectrometer) in the wavenumber range from 400 to 4000 cm^{-1}. To obtain the IR spectra, a ratio of 1:100 of the sample and potassium bromide, KBr were used. The background using a control sample of KBr was always taken prior to each measurement. The applied resolution and number of scan was 4 cm^{-1} and 100 per minute, respectively. TG and DSC analysis were performed at room temperature 25 ^{0}C to 1000 ^{0}C at a heating rate of 10 ^{0}C /min under argon gas flow by a NETZSCH Thermal Analysis STA 449C. A QuantaMaster ™ 510 spectrofluorometer (HORIBA Jobin Yvon GmbH, Germany) was used to record photoluminescence spectra at room temperature with excitation wavelength, λ_{ex} = 300 nm.

3. Results and discussion

3.1. XRD analysis

Fig. 2 illustrates the X-ray diffraction patterns of La_2O_3 NPs prepared with PEG concentration of 60 g/l calcined at 750 ^{0}C, 900 ^{0}C and 1000 ^{0}C, and all these X-ray diffraction patterns reveal the overall crystal structure and phase purity of the La_2O_3 NPs. The diffraction peaks of all samples were indexed to (100), (002), (101), (102), (110), (200), (112), and (201) reflections corresponding to the pure hexagonal phase with lattice constant, $a = b$ = 0.3973 nm and c = 0.6129 nm (JCPDS card No. 83-1348). The strong and sharp diffraction peaks of all samples confirm the good crystallinity of the La_2O_3 NPs. The broader peaks suggest the nanometer-sized structures of the La_2O_3 NPs. It is observed that with increasing calcination temperature from 750 ^{0}C to 1000 ^{0}C the height of the peak increases and full width at half maximum (FWHM) decreases, that is diffraction peaks become stronger and sharper indicating the crystallinity of the samples improve and the size of particles getting larger [36, 37].

The lattice constants, a, b and c of the unit cell for hexagonal structure of La_2O_3, were calculated by the following equation [39]:

$$\frac{1}{d^2_{\square kl}} = \frac{4}{3}\left(\frac{\square^2 + \square k + k^2}{a^2}\right) + \frac{l^2}{c^2} \qquad (1)$$

where d_{hkl} is the interplanar spacing of the atomic planes and hkl is Miller indices. The calculated values of *a*, *b* and *c* is listed in Table 1. The obtained results are well agreement with the reported values [40].

The width of the diffraction peak varies with the crystallite size of the material. The crystallite size, *D* of sample material can be estimated by using the Scherrer's formula [41]:

$$D = \frac{M\lambda}{\beta cos\theta_B} \qquad (2)$$

where *D* is the diameter of the crystallite, β is the FWHM of the selected diffraction peak, θ_B is the Bragg angle, λ is the wavelength of the X-ray used, and *M* is a constant of which the value depends on the shape of the crystallite.

The FWHM of the XRD peaks may also contain contributions from lattice strain, ε_{str} and the strain induced in powders owing to crystal imperfection and distortion can be calculated by using the Stokes-Wilson equation [42]:

$$\varepsilon_{str} = \frac{\beta_C}{4\ tan\theta} \qquad (4)$$

The values of average crystallite size and lattice strain determined by using Equations (3) and (4) and values are tabulated in Table 2. It is observed from the data in the Table 2 that the average crystallite size decreases while lattice strain increases with increasing concentration of PEG in the sol. On the contrary, average crystallite size increases while lattice strain decreases with increasing calcination temperature. The similar result was reported by Wang *et al.* [36].

A variety of properties of the materials is strongly affected by crystallographic defects or irregularity within a crystal structure. This defects or irregularity is known as dislocation. The dislocation density, δ for La_2O_3 NPs can be determined by the expression [43]:

$$\delta = \frac{15\beta\ cos\theta}{4aD} \qquad (5)$$

In crystalline solids, atoms or molecules exist in a periodic nature and repeat fixed distance positions, called unit cell parameter. The unit cell volume, *V* for hexagonal La_2O_3 NPs can be calculated by the relation below [44]:

$$V = \frac{\sqrt{3}}{2}a^2c \qquad (6)$$

The calculated values of δ and *V* for all samples are listed in Table 2.

The crystalinity of the sample material can be represented by the crystal index, C_i and can be calculated by the following equation [35]:

$$C_i = \frac{I_{max}}{\beta_c} \qquad (7)$$

In this case I_{max} is the maximum intensity of the XRD peak and β_c is the value of corrected FWHM.

The obtained value of dislocation density, unit cell volume and crystal index are listed in Table 2. It is found that dislocation density is higher for samples calcined at 900 ^{0}C presenting the higher concentration of crystal imperfections in the samples. It is apparent that samples calcined at temperature 1000 ^{0}C have larger unit cell volume as compared to the other samples.

3.2 Surface Morphology and Particle Size Measurement

Fig. 3, Fig. 4 and Fig. 5 show SEM micrographs of dispersed La_2O_3 NPs prepared with PEG concentration of 60 g/l calcined at 750 ^{0}C, 900 ^{0}C and 1000 ^{0}C, respectively at different magnifications. In this case, to get average crystallite size for every sample, at least ten crystallites were considered and their diameter were measured from a software connected with ESEM which was marked in every samples. The nanoparticles were dispersed in ethanol with the help of an ultrasonic bath (probe power level 3 and power density of 0.275 W/mL) for 20 min. From all Figures, it can be seen that the La_2O_3 NPs are uniformly dispersed and mostly spherical in shape with diameters from approximately 32 nm to 56 nm. This can be attributed to the fact that the acoustic waves transmitted by ultra-sonication are effective in dispersing La_2O_3 NPs owing to the transient cavitations and acoustic streaming that can possibly redefine the shape and structure of NPs and change the surface morphology [45]. From the results [shown in supplementary Figures], it can be seen that the particle size of the as synthesized La_2O_3 NPs decreased with increasing PEG concentration. This can be attributed to the enhanced steric hindrance by the adsorption of polymer polyethylene glycol on the surfaces of lanthanum oxide particles. That is the polyethylene glycol polymer surrounds the crystal nuclei of lanthanum nitrate and prevents their growth which creates steric hindrance effect resulting to reduce particle-particle aggregation. When the concentration of PEG is not enough to fully cover the crystal nuclei, the growth of crystal is not impeded effectively by adsorbing PEG. As a result, bigger particles will be acquired. On the other hand, if the concentration of PEG rises, then the coverage degree of PEG on the crystal nuclei will increase and consequently average particle size is thinly decreased. At the same time, the particle-particle agglomeration is gradually reduced [36].

The change of the average particle size with calcinations temperature is summarized in Table 3 to understand the influence of particle size on the calcination temperature clearly. It can be concluded from the result shown in Table 3 that the particle size is gradually increased with the increase in calcination temperatures. This is fact can be explained as that at low temperature the particles grow gently while at higher temperature particles grow very rapidly to form agglomeration. The similar type of results was found by earlier researchers [36].

3.3 Chemical Composition Study

The EDS spectra of NPs La_2O_3 NPs prepared with PEG concentration of 60 g/l calcined at 750 ^{0}C, 900 ^{0}C and 1000 ^{0}C are represented in Fig. 6, respectively. The EDS spectrum shows presence of lanthanum, oxygen, carbon, and platinum. The small carbon peak was originated from the tiny carbon tape mounted on a stainless steel stab which was applied during the sample preparation for SEM. The Pt peak was resulted from platinum coating of the samples which was used to make the sample highly conductive. The weight percentage (wt. %) of the different elements present in all samples are listed in Table 4. It is observed from the results shown in Table 4, that highest weight percentage of Lanthanum (La) is present in the sample while a good amount of Oxygen (O) is also observed. The theoretical percentage of lanthanum in La_2O_3 NPs is 85.3% and that of oxygen is 14.73 % while the EDX results showed on the average 75.03 % of lanthanum and 19.76 % of oxygen. These obtained results confirmed a good agreement with previous work [35]. The EDX analysis indicates no presence of any impurity.

3.4 Thermal analysis of La_2O_3 NPs

Fig. 7 illustrates the TG-DSC curves of the lanthanum dried gel powder prepared at PEG concentration of 60 g/l. The thermogram of Fig. 7 shows four different regions indicated by letter A, B, C and D. These regions are indication of different weight losses of the sample at different range of temperature. The weight loss approximately 1.5 % in the first region (A) between temperature 30 to 250 ^{0}C corresponds to the removal of surface absorbed water of the sample and because of this a small endothermic peak in DSC curve is obtained at about 95 ^{0}C. In the second region (B) between temperature 250-400 ^{0}C, DSC curve indicates a sharp endothermic peak at 380^{0}C and the corresponding weight loss in the in this region is 8.25 %. This can be explained as the evaporation of the surfactant (PEG), whose boiling point is 260 ^{0}C. The weight loss (2.75 %) in the third region, C is due to the oxidation of the residual organic compounds from surfactant, PEG. A small endothermic peak in this region at a temperature 510 ^{0}C is also observed. Finally, in the fourth region (D) an endothermic peak at 750 ^{0}C in DSC curve is obtained and the corresponding weight loss in this region is around 3.5 %. This is because of the final decomposition of lanthanum

compound of the sample [36]. That is, PEG and all others lanthanum compound of the sample decomposed completely at 750 °C. Hence, 750 °C was chosen as the minimum calcination temperature.

3.5 Fourier Transform Infrared Spectroscopy analysis

The FTIR spectra in the wavenumber range 4000-400 cm^{-1} of the as-prepared La_2O_3 NPs samples are depicted in Fig. 8. At the spectrums of the samples with PEG concentration of 60 g/l calcined at 750 ^{0}C, 900 ^{0}C and 1000 ^{0}C in Fig. 8, a broad band is observed at the wavenumber of 3439 cm^{-1} (A), 3424 cm^{-1} (A) and 3442 cm^{-1}(A), respectively and these bands show the presence of O-H stretching vibration which is due to absorbed moisture on the surface of the samples [36]. The absorption peaks at around 1459, 1460 and 1464 cm^{-1} (B) as well as sharp absorption bands at 1362, 1363 and 1363 cm^{-1} (C) in the samples is found because of the asymmetric and symmetric stretching of COO^-, respectively [37]. The band at 1067 cm-1 (D) in three samples is for C-O stretching vibration but in the same samples, the sharp absorption bands at around 856 cm^{-1}(E) is owing to C-O bending vibration. The broad absorption bands at 648, 678 and 663 cm^{-1}(F) in three samples is observed because of the La-O stretching vibration while the small bands at 510, 510 and 514 cm^{-1}(G) in the same samples is due to La–O bending vibration. The presence of above mentioned bands therefore confirmed the existence of La_2O_3 [38]. The location of all the band frequencies and their corresponding modes of vibration are recorded in Table 5 for better comparison.

3.6 Photoluminescence Spectroscopy Study

The Photoluminescence (PL) spectra of different La_2O_3 NPs samples are illustrated in Fig. 9. From Figures 9 it is seen that the strongest emission band is found to be located at the wavelength of 364 nm for all samples. The observed emission band at 364 is a typical green band. This may be ascribed to recombination of a delocalized electron near to the conduction band with a single charged state of a surface oxygen vacancy [46]. The higher fluorescence intensity of the La_2O_3 sample is an indication of the higher surface-to-volume ratio and due to higher density of single ionized oxygen vacancies, resulting from the small particle size as has been suggested by G. Wang *et al.* [47]. A small band is also observed at 465 nm for all samples.

4. Conclusions

La_2O_3 nanoparticles were successfully synthesised via a simple sol-gel technique and the effect of calcinations temperature on the size of nanoparticles was also investigated. All of the diffraction peaks of La_2O_3 NPs obtained from XRD data were indexed to (100), (002), (101), (102), (110),(200), (112), and (201) reflections corresponding to the pure hexagonal phase. The average crystal size calculated by the Debye Scherrer's equation was found to be in the range of 18.14-29.31 nm while that of estimated from ESEM micrographs for different dispersed La_2O_3 NPs samples were found from 32.59 nm to 55.73 nm. The particle size was found to be increased with increasing calcination temperature while that of decreased with increasing concentration of the PEG in the solution. The EDS study confirmed the presence of Oxygen and Lanthanum in the synthesized nanoparticles. The thermograms of all samples showed three main thermal transitions associated with weight loss. The FTIR spectroscopy suggested that all samples exhibited a broad band in the range of 3442-3424 cm^{-1} associated with O-H stretching vibrations in absorbed water molecules. Absorption bands in the frequency range 1067 cm^{-1}associated with C-O stretching vibrations where observed, while C-O bending vibrations appeared in the range of 856-845 cm^{-1}. La-O stretching and bending vibrations were observed in the wavenumber range of 678-648 cm^{-1} and 514-510 cm^{-1}, respectively. The Photoluminescence spectra of different samples of La_2O_3 NPs presented a strong emission band located at the wavelength of 364 is typical green band.

Conflict of interest statement

The authors declare that they have no conflict of interest.

Acknowledgments

The author (H. Kabir) acknowledged gratefully for the financial support of Bangladesh Government under Bangabandhu Fellowship. He also acknowledges thankfully Jahangirnagar University, Bangladesh for providing the required study leave to carry out this work at School of Metallurgy and Materials, University of Birmingham, UK.

References

[1] P. Huang, J. Li, S. Zhang, C. Chen, Y. Han, N. Liu, Y. Xiao, H. Wang, M. Zhang, Q. Yu, Y. Liu, and W. Wang, Effects of lanthanum, cerium, and neodymium on the nuclei and

mitochondria of hepatocytes: Accumulation and oxidative damage, Environ. Toxicol. Pharmacol. 31 (2011) 25–32.

[2] Z. K. Bolaghi, S. M. Masoudpanah, M. Hasheminiasari, Photocatalytic properties of ZnO powders synthesized by conventional and microwave-assisted solution combustion method, J. Sol-Gel Sci Technol. 86 (2018) 711-718.

[3] M. H. Oghaz, R. S. Razavi, M. Barekat, M. Naderi, S. Malekzadeh, M. Rezazadeh, Synthesis and characterization of Y2O3 nanoparticles by sol–gel process for transparent ceramics applications, J. Sol-Gel Sci. Technol. 78 (2016) 682–691.

[4] Y. Xin, Y. Qi, X. Ma, Z. Wang, Z. Zhang, and S. Zhang, Rare-earth (Nd, Sm, Eu, Gd and Y) enhanced CeO_2 solid solution nanorods prepared by co-precipitation without surfactants, Mater. Lett. 64 (2010) 2659–2662.

[5] G. Oskam, Metal oxide nanoparticles: synthesis, characterization and application, J. Sol-Gel Sci Techn. 37 (2006) 161-164.

[6] A. H. Lu, E. L. Salabas, and F. Schüth, "Magnetic nanoparticles: Synthesis, protection, functionalization, and application, Angew. Chemie - Int. Ed. 46 (2007) 1222–1244.

[7] J. Das, V. S. Moholkar, S. Chakma, Structural, magnetic and optical properties of sonochemically synthesized Zr-ferrite nanoparticles, Powder Technol. 328 (2018) 1-6.

[8] C. Aubery, C. Solans, S. Prevost, M. Gradzielski, and M. Sanchez-Dominguez, Microemulsions as reaction media for the synthesis of mixed oxide nanoparticles: Relationships between microemulsion structure, reactivity, and nanoparticle characteristics, Langmuir 29 (2013) 1779–1789.

[9] N. C. Zheng, Z. Wang, J. Y. Long, L. J. Kong, D. Y. Chen, Z. Q. Liu, Shape-Dependent Adsorption of CeO2 Nanostructures for Superior Organic Dye Removal, J. Colloid Interface Sci. 525 (2018) 225–233.

[10] H. Abdulhamid, E. Fridell, and M. Skoglundh, Influence of the type of reducing agent (H_2, CO, C_3H_6 and C_3H_8) on the reduction of stored NOX in a Pt / BaO / Al_2O_3 model catalyst, 2004 (2010) 161–168.

[11] S. F. Hasany, I. Ahmed, R. J, and A. Rehman, Systematic Review of the Preparation Techniques of Iron Oxide Magnetic Nanoparticles, Nanosci. Nanotechnol. 2 (2012) 148–158.

[12] E. K. Goharshadi, S. H. Sajjadi, R. Mehrkhah, and P. Nancarrow, Sonochemical synthesis and measurement of optical properties of zinc sulfide quantum dots, Chem. Eng. J. 209 (2012) 113–117.

[13] E. K. Goharshadi and H. Azizi-Toupkanloo, Silver colloid nanoparticles: Ultrasound-assisted synthesis, electrical and rheological properties, Powder Technol. 237 (2013) 97–

101.

[14] Y. Gao, Y. Masuda, and K. Koumoto, Micropatterning of lanthanum-based oxide thin film on self-assembled monolayers, J. Colloid Interface Sci. 274 (2004) 392–397.

[15] L. Zhang, L. Zhou, Q. X. Li, H. Liang, H. Qin, S. Masutani, B. Yoza, Toxicity of lanthanum oxide nanoparticles to the fungus Moniliella wahieum $Y12^T$ isolated from biodiesel, Chemosphere 199 (2018) 495-501.

[16] J. Kang, Y. Kim, D. W. Cho, Y. Sohn, Synthesis and physicochemical properties of $La(OH)_3$ and La_2O_3 nanostructures, Mater. Sci. Semicon. Proces. 40 (2015) 737–743.

[17] S. Khanjani and A. Morsali, Synthesis and characterization of lanthanum oxide nanoparticles from thermolysis of nanostructured supramolecular compound, J. Mol. Liq. 153 (2010) 129–132.

[18] J. Liu, G. Wang, L. Lu, Y. Guo and L. Yang, Facile shape-controlled synthesis of lanthanum oxide with different hierarchical micro/nanostructures for antibacterial activity based on phosphate removal, RSC Adv. 7 (2017), 40965-40972.

[19] C. C. Li, M. J. Li, Y. P. Huang, Dispersion of aluminum-doped zinc oxide nanopowder with high solid content in ethylene glycol, Powder Technol. 327 (2018) 1-8.

[20] A. V. Murugan, S. C. Navale, V. Ravi, Synthesis of nanocrystalline La_2O_3 powder at 100 °C, Mater. Lett. 60 (2006) 848–849.

[21] A. Bahari, A. Anasari and Z. Rahmani, Low temperature synthesis of La_2O_3 and CrO_2 by Sol – Gel process, J. Engi. Technol. Res. 3(2011) 203-208.

[22] S. Jafari Nejad, H. Abolghasemi, M. a. Moosavian, A. Golzary, and M. G. Maragheh, Fractional factorial design for the optimization of hydrothermal synthesis of lanthanum oxide nanoparticles under supercritical water condition, J. Supercrit. Fluids 52 (2010) 292–297.

[23] J. Sheng, S. Zhang, S. Lv, W. Sun, Surfactant-assisted synthesis and characterization of lanthanum oxide nanostructures, J. Mater. Sci. 42 (2007) 9565–9571.

[24] M. Salavati-Niasari, G. Hosseinzadeh, and F. Davar, Synthesis of lanthanum hydroxide and lanthanum oxide nanoparticles by sonochemical method, J. Alloys Compd. 509 (2011) 4098–4103.

[25] M. Ranjbar and M. Yousefi, Synthesis and Characterization of Lanthanum Oxide Nanoparticles from Thermolysis of Nano-sized Lanthanum(III) Supramolecule as a Novel Precursor, J. Inorg. Organomet. Polym. Mater. 24 (2014) 652–655.

[26] S. Wang, Y. Zhao, J.Chen, R. Xu, L. Luo, S. Zhong, Self-assembled 3D $La(OH)_3$ and La_2O_3 nanostructures: Fast microwave synthesis and characterization, Superlattices and Microstructures 47 (2010) 597−605.

[27] B. Tang, J. Ge, C. Wu, L. Zhuo, J. Niu, Z. Chen, Z. Shi, and Y. Dong, Sol–solvothermal synthesis and microwave evolution of $La(OH)_3$ nanorods to La_2O_3 nanorods This, Nanotechnol. 15 (2004) 1273–1276.

[28] M. F. Vignolo, S. Duhalde, M. Bormioli, and G. Quintana, Structural and electrical properties of lanthanum oxide thin films deposited by laser ablation, Appl. Surf. Sci. 197 (2002) 522–526.

[29] M. Ghiasi, A. Malekzadeh, Synthesis, characterization and photocatalytic properties of lanthanum oxy-carbonate, lanthanum oxide and lanthanum hydroxide nanoparticles, Superlattices and Microstructures 77 (2015) 295–304.

[27] J. Zhu, Z. Gui, and Y. Ding, A simple route to lanthanum hydroxide nanorods, Mater. Lett. 62 (2008) 2373–2376.

[28] G. Guo, F. Gu, Z. Wang, and H. Guo, Synthesis and characterization of $La_2(CO_3)_3$ nanostructures in the Triton X-100/cyclohexane/water reverse micelles, J. Cryst. Growth 277 (2005) 631–635.

[29] M. A. Farrukh, F. Imran, S. Ali, M. K. Rahman and I. I. Naqvi, Micelle Assisted Synthesis of La_2O_3 Nanoparticles and Their Applications in Photodegradation of Bromophenol Blue, Russian J. Appl. Chem. 88 (2015) 1523−1527.

[30] Q. L. Zhang, Z. J. Ji, J. Zhou, X. C. Zhao, X. Z. Lan, Preparation of Lanthanum Oxide Nanoparticles by Chemical Precipitation Method, Mater. Sci. Forum, 724 (2012) 233-236.

[31] M. A. Farrukh, F. Imran, S. Ali, M. K. Rahman and I. I. Naqvi, Micelle Assisted Synthesis of La_2O_3 Nanoparticles and Their Applications in Photodegradation of Bromophenol Blue, Russian J. Appl. Chem. 88 (2015) 1523−1527.

[32] C. Wang, Y. Yang, Z. Zhang, F. Liao, J. Ju, Z. Shi, J. Lin, Y. Li, F. Huang, Synthesis of nano-structured La_2O_3/$La_2O_2CO_3$:Eu phosphors from arc-discharged graphene-contained composites, Mater. Lett. 134 (2014)176–179.

[33] Y. Xiao, Z. Feng, X. Huang, L. Huang, Z. Long, Q. Wang,Y. Hou, Synthesis of lanthanum oxide nanosheets by a green carbonation process, Chin. Sci. Bull. 59 (2014)1864–1867.

[34] M. Moothedan, K.B. Sherly, Synthesis, characterization and sorption studies of nano lanthanum oxide, J. Water Process Engi. 9 (2016) 29–37.

[35] E. K. Goharshadi, T. Mahvelati, and M. Yazdanbakhsh, Influence of preparation methods of microwave, sol–gel, and hydrothermal on structural and optical properties of lanthania nanoparticles, J. Iran. Chem. Soc. 13 (2016) 65–72.

[36] X. Wang, M. Wang, H. Song, and B. Ding, A simple sol-gel technique for preparing lanthanum oxide nanopowders, Mater. Lett. 60 (2006) 2261–2265.

[37] M. S. Niasaria, G. Hosseinzadeh, F. Davar, Synthesis of lanthanum carbonate nanoparticles

via sonochemical method for preparation of lanthanum hydroxide and lanthanum oxide nanoparticles, J. Alloys Compd. 509 (2011) 134–140.

[38] Q. Zhou, H. Zhang, F. Chang, H. Li, H. Pan, W. Xue, D.Y. Hu, S. Yang, Nano La_2O_3 as a heterogeneous catalyst for biodiesel synthesis by transesterification of Jatropha curcas L. oil, J. Indust. Eng. Chem. 31(2015) 385–392.

[39] G. Z. Jia, Y. F. Wang, and J. H. Yao, Fabrication and strain investigation of ZnO nanorods on Si composing sol-gel and chemical bath deposition method, J. Phys. Chem. Solids. 73 (2012) 495–498.

[40] C. Hu, H. Liu, W. Dong, Y. Zhang, G. Bao, C. Lao, Z. L. Wang, $La(OH)_3$ and La_2O_3 Nanobelts—Synthesis and Physical Properties, Adv. Mater. 19 (2007) 470–474.

[41] B. D. Cullity, Elements of X-ray Diffraction, Second Ed., Addison-Wesley Company, USA, 1978.

[42] R. Jenkins, R. L. Snyder, Chemical Analysis: Introduction to ray Powder Diffractometry, John Wiley & Sons, Inc., New York, 1996.

[43] R. John, and R. Rajakumari, Synthesis and Characterization of Rare Earth Ion Doped Nano ZnO, Nano-Micro Lett. 4 (2012) 65-72.

[44] F. Ozutok, B. Demirselcuk, E. Sarica, S. Turkyilmaz, V. Bilgin, Study of Ultrasonically Sprayed ZnO Films: Thermal Annealing Effect, Acta Phys. Polonica. A, 121 (2012) 53-55.

[45] D. Dickson, G. Liu, C. Li, G. Tachiev, Y. Cai, Dispersion and stability of bare hematite nanoparticles: Effect of dispersion tools, nanoparticle concentration, humic acid and ionic strength, Sci. Total Environ. 419 (2012) 170–177.

[46] N. Zhang, R. Yi, L. Zhou, G. Gao, R. Shi, G. Qiu, X. Liu, Lanthanide hydroxide nanorods and their thermal decomposition to lanthanide oxide nanorods, Mater. Chem. Phys. 114 (2009) 160–167.

[47] G. Wang, Y. Zhou, D. G. Evans, and Y. Lin, Preparation of Highly Dispersed Nano-La_2O_3 Particles Using Modified Carbon Black as an Agglomeration Inhibitor, Ind. Eng. Chem. Res. 51 (2012) 14692−14699.

Figure

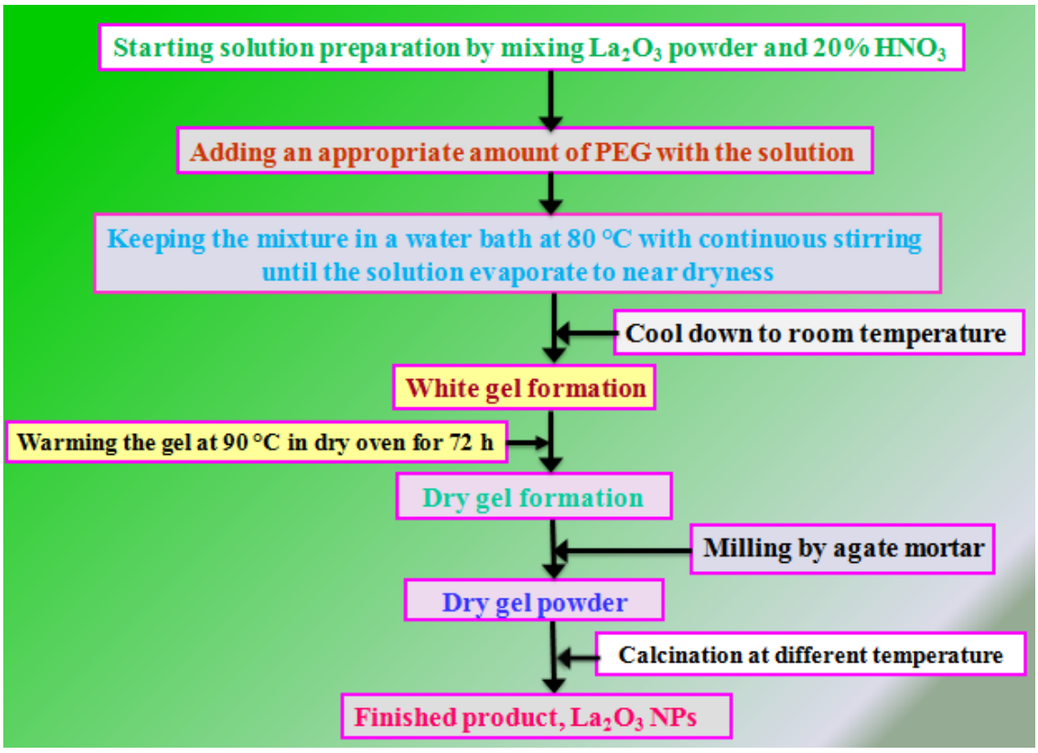

Fig. 1. Flow chat for the synthesis of La_2O_3 NPs via sol-gel technique.

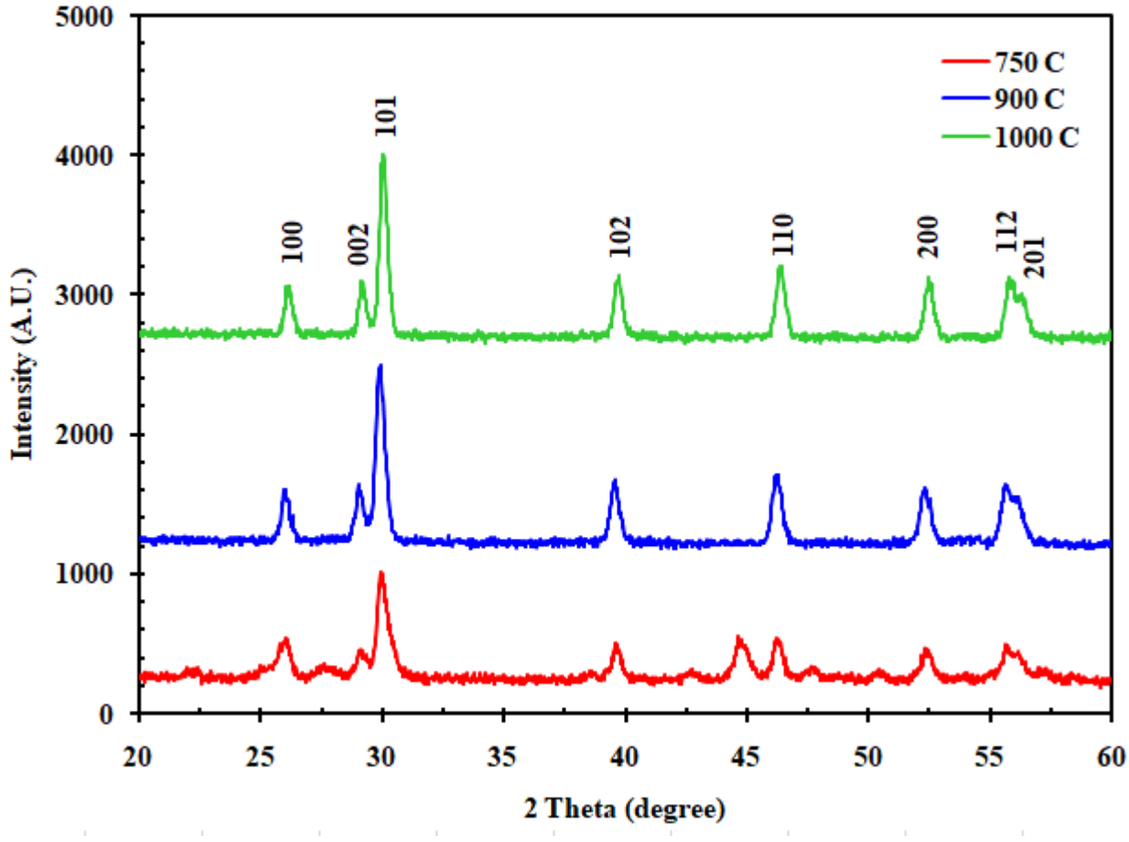

Fig. 2. XRD patterns of La_2O_3 NPs samples calcined at 750 ^{0}C, 900 ^{0}C and 1000 ^{0}C [PEG concentration 60 g/l].

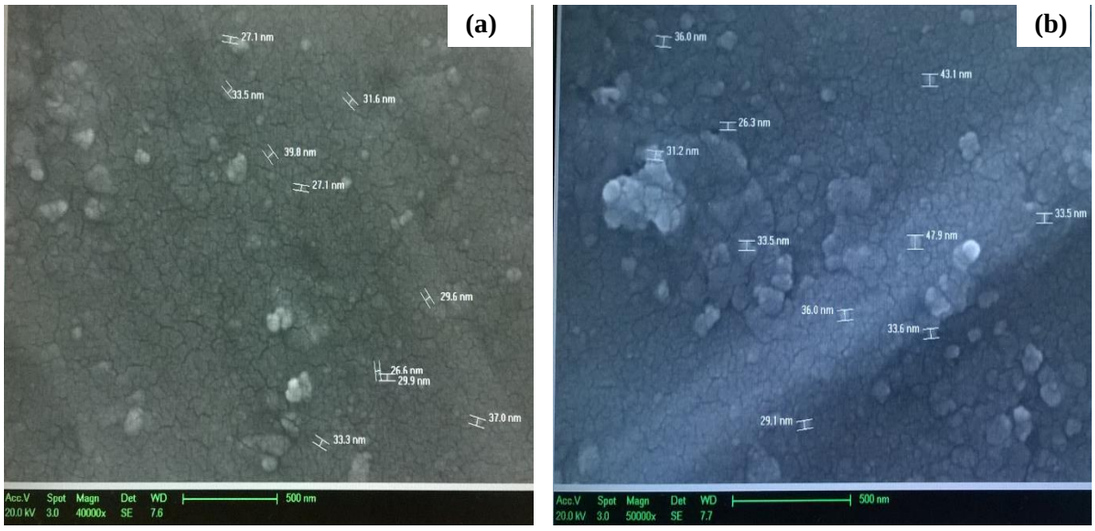

Fig. 3: SEM micrographs of dispersed La_2O_3 NPs sample calcined at 750 ^{0}C, at magnification (a) 40k×, (b) 50k×.

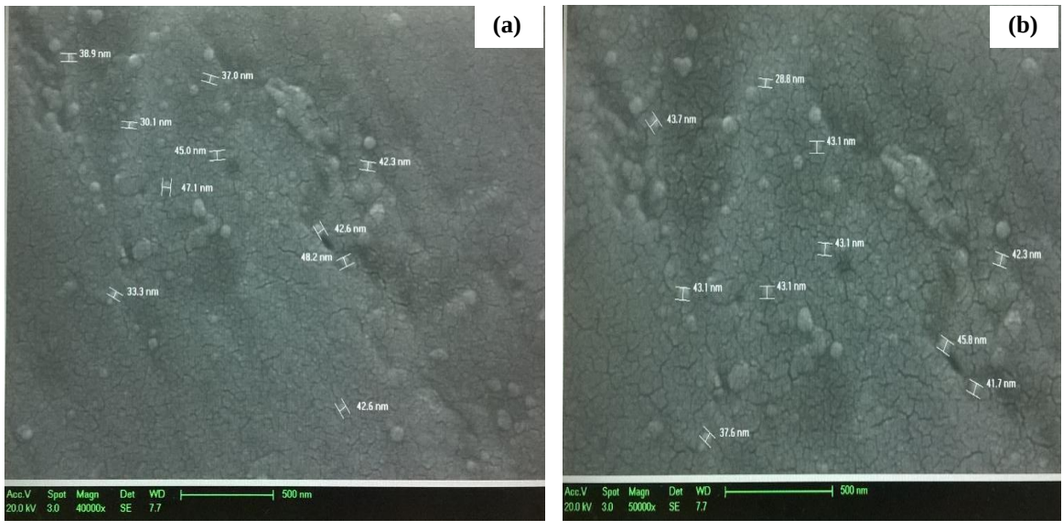

Fig. 4: SEM micrographs of dispersed La_2O_3 NPs sample calcined at 900 ^{0}C, at magnification (a) 40k×, (b) 50k×.

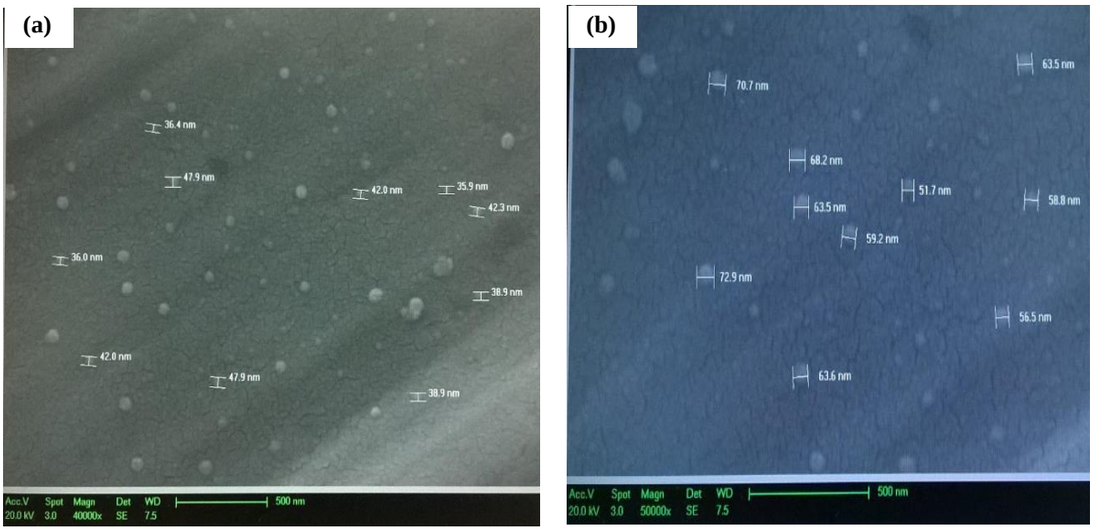

Fig. 5: SEM micrographs of dispersed La_2O_3 NPs sample calcined at 1000 ^{0}C, at magnification (a) 40k×, (b) 50k×.

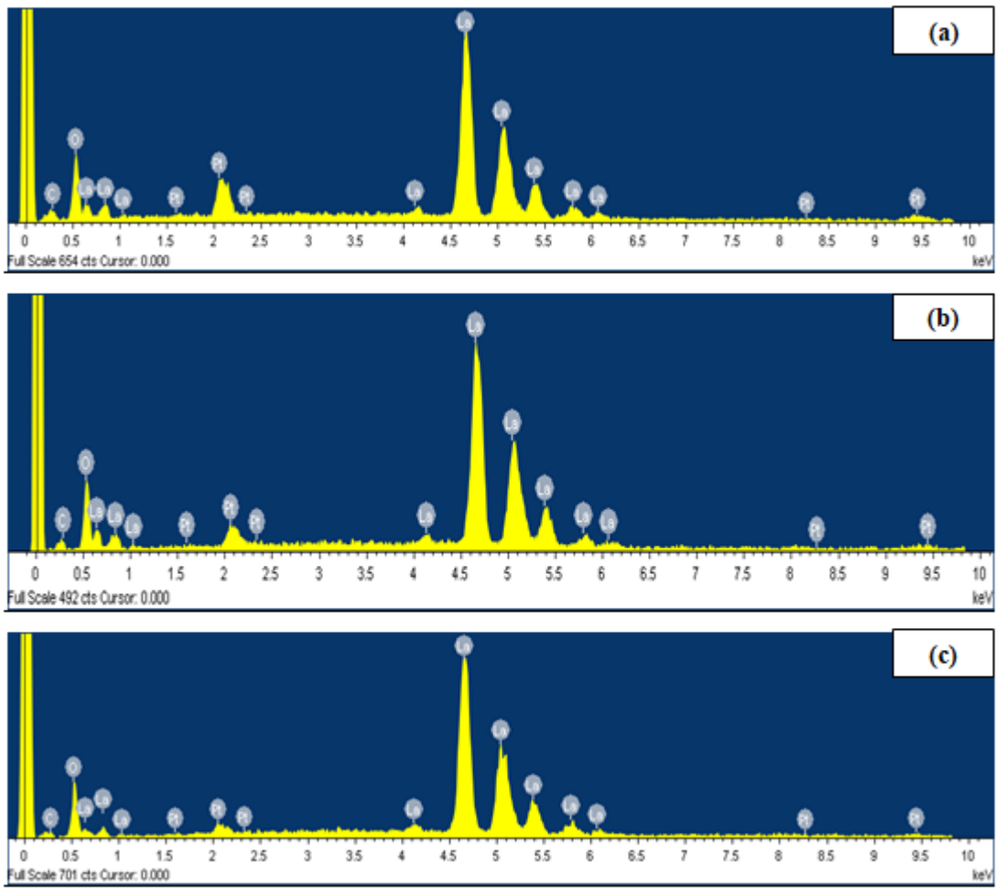

Fig. 6: EDS spectra of La_2O_3 NPs samples calcined at 750 ^{0}C, 900 ^{0}C and 1000 ^{0}C [PEG concentration 60 g/l].

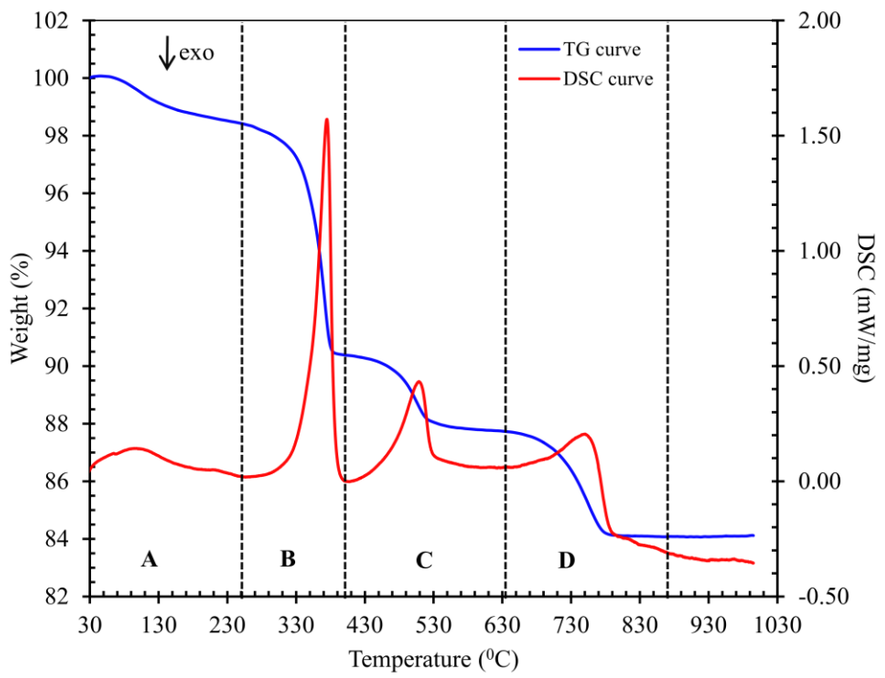

Fig. 7: TG-DSC traces of the lanthanum compound dried gel powder prepared at PEG concentration of 60 g/l.

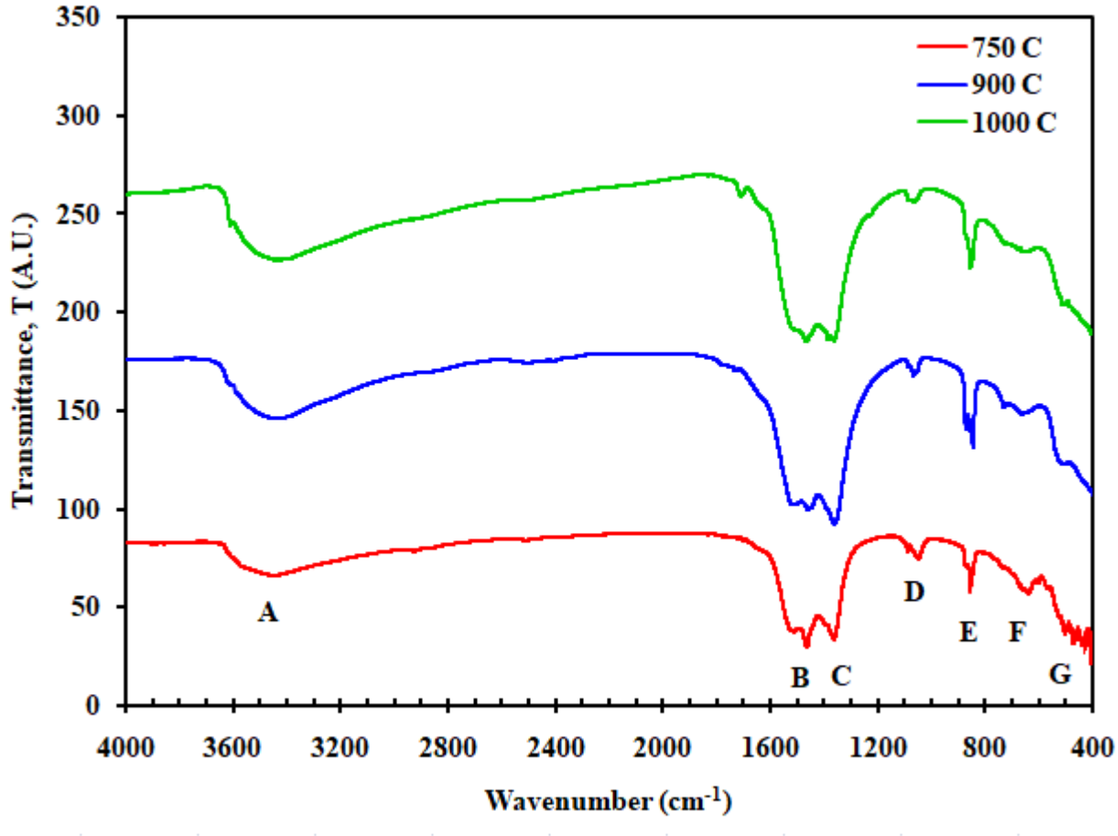

Fig. 8: FTIR spectra of La_2O_3 NPs samples calcined at 750 ^{0}C, 900 ^{0}C and 1000 ^{0}C [PEG concentration 60 g/l].

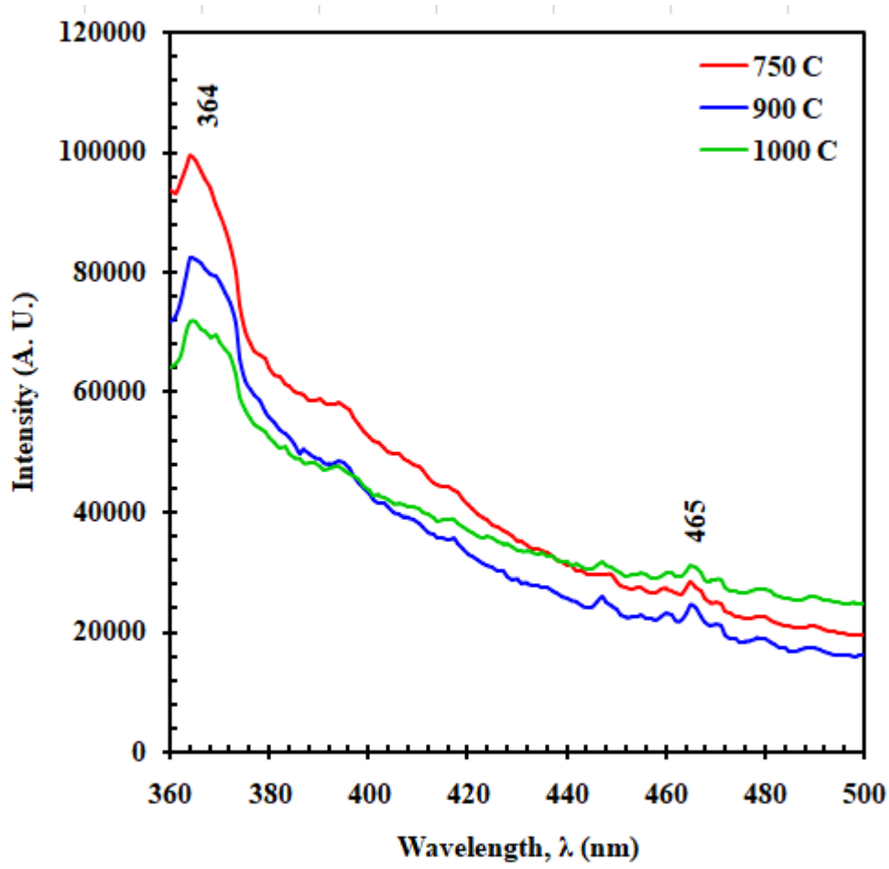

Fig. 9: PL spectra of La_2O_3 NPs samples calcined at 750 ^{0}C, 900 ^{0}C and 1000 ^{0}C [PEG concentration 60 g/l].

Table

Table 1. Determination of interplanar distance and lattice constants of La_2O_3 NPs.

Sample (Calcination Temp.)	Interplanar distance, d_{hkl} (Å)			Lattice constants, a and b (Å)			Lattice constants, c (Å)			Average values of a or b (Å)	Average of c (Å)
	(100)	(002)	(110)	(100)	(002)	(110)	(100)	(002)	(110)		
750 ^{0}C	3.4219	3.0688	1.9630	3.9513	3.9397	3.9260	6.0801	6.1377	6.2081	3.9390	6.1420
900 ^{0}C	3.4144	3.0750	1.9595	3.9426	3.9274	3.9190	6.0741	6.1499	6.1936	3.9297	6.1392
1000 ^{0}C	3.4174	3.0664	1.9595	3.9461	4.0885	3.9190	6.057	6.1328	6.1936	3.9845	6.1278

Table 2. Crystallographic parameters of La_2O_3 NPs.

Sample	Crystallite size, D (nm)	Lattice strain, ε	Dislocation density, δ	Unit cell volume, V(Å^3)	Crystal index, C_i	c/a ratio
750 ^{0}C	18.14	0.0077	0.0240	82.5274	1561.16	1.5593
900 ^{0}C	25.37	0.0055	0.1081	82.0993	4056.49	1.5623
1000 ^{0}C	29.31	0.0048	0.0089	84.2509	3775.58	1.5379

Table 3. Average particle size for different dispersed samples of La_2O_3 NPs:

Sample	Magnification(k×)	Particle size (nm)	Average particle size (nm)
750 ^{0}C	40	31.55±3.49	32.59±4.04
	50	35.02±4.58	
900 ^{0}C	40	40.81±4.59	41.71±3.90
	50	41.23±3.21	
1000 ^{0}C	40	40.82±3.60	55.73±4.32
	50	62.86±5.05	

Table 4. The weight percentage (wt. %) of the different elements present in different samples of La_2O_3 NPs.

Sample	Element present in Wt%		
	La	O	C
750 ^{0}C	67.81	25.23	6.96
900 ^{0}C	69.83	24.04	6.13
1000 ^{0}C	80.20	15.92	3.88

Table 5. Assignments of FTIR absorption peaks for La_2O_3 nanoparticles samples.

Assignments	Wavenumber (cm^{-1})		
	As prepared La_2O_3 nanoparticles		
	750 ^{0}C	900 ^{0}C	1000 ^{0}C
O-H stretching vibration (A)	3439	3424	3442
Asym. stretching of COO^- (B)	1509, 1459	1510, 1460	1464
Symmetric stretching of COO^- (C)	1362	1363	1363
C-O stretching vibration (D)	1067	1067	1067
C-O bending vibration (E)	856, 845	856, 845	855
La-O stretching vibration (F)	648	678	663
La–O bending vibration (G)	510	510	514

UNIVERSITY OF BIRMINGHAM

COLLEGE OF ENGINEERING AND PHYSICAL SCIENCES

School of Metallurgy and Materials

Birmingham B15 2TT, UK
Phone: +44 121 414 3344

The Editor

Journal of Applied Physics A

Submission of Full-Length Article to Journal of Applied Physics A

With reference to the above, I attach herewith an article entitled "Influence of Calcination on Sol-Gel Synthesis of lanthanum oxide nanoparticles" for submission to ***Journal of Applied Physics A*** as a full-length research paper.

Authors are ensuring that this is an original article. The article has been written by the stated authors who are ALL aware of its content and all authors have approved the final article. We would like to assure the publisher that this work has not been published/submitted or being submitted to another journal or is not under consideration for publication elsewhere. Authors also declared that no conflict of interest exists for this article. Authors also confirming that if accepted, the article will not be published elsewhere in the same form, in any language, without the written consent of the publisher. It is also assured to the publisher that this manuscript was not previously submitted to ***Journal of Applied Physics A***. All the authors mutually agree to submission of the manuscript to ***Journal of Applied Physics A*** and assign to *Springer Link* the copyright if the article is accepted for publication.

We appreciate your kind action on for publishing this paper at your esteemed journal.

Thank you,

Yours sincerely,

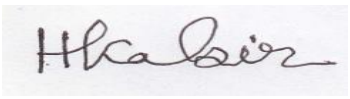

Humayun Kabir
Corresponding author
Email: rumy140@juniv.edu